Hindawi
International Transactions on Electrical Energy Systems
Volume 2022, Article ID 4332766, 15 pages
https://doi.org/10.1155/2022/4332766

Research Article

Wearable Mixed Energy Management System Based on Power Trajectory Tracking

Shijun Shen,[1] Chaofan Wang,[1] Chuan Lu,[2] Wei Zheng,[3] and Dawei Gong[1]

[1]*University of Electronic Science and Technology of China, Chengdu 611731, China*
[2]*Science and Technology on Reactor System Design Technology Laboratory, Nuclear Power Institute of China, Chengdu 610213, China*
[3]*Science and Technology on Thermal Energy and Power Laboratory, Wuhan Second Ship Design and Research Institute, Wuhan 430064, China*

Correspondence should be addressed to Dawei Gong; pzhzhx@126.com

Received 30 March 2022; Accepted 21 April 2022; Published 1 June 2022

Academic Editor: Qiuye Sun

Copyright © 2022 Shijun Shen et al. This is an open access article distributed under the Creative Commons Attribution License, which permits unrestricted use, distribution, and reproduction in any medium, provided the original work is properly cited.

With more and more extensive research and application of wearable devices, their continuous working time has become a prominent problem which is increasingly concerned. Within the limitations of existing battery technology, environmental energy harvesting can be used to enhance the continuous working time of wearable devices. To solve this problem, this paper designs a collection system for heat energy and radiofrequency (RF) energy in the environment. This system designs a thermoelectric collector based on thermoelectric generation, an RF energy collector based on a rectifier antenna, and a mixed energy collection controller based on power trajectory tracking. This system can generate power according to the temperature difference between environment and human body and RF energy in the environment. This system uses the heart rate sampling algorithm to accurately collect the required voltage and current information while saving system energy consumption. The maximum power output algorithm based on power trajectory tracking keeps the maximum power output of the energy collection system at all times. In this paper, two kinds of environmental energy models and a mixed energy acquisition system model are established by MATLAB. After setting reasonable environmental conditions, we get the results to verify the rationality and effectiveness of this environment energy collection system.

1. Introduction

As the material basis of human production, energy has been playing an important role in the development of human society. The energy collection technology is to collect the energy lost in the environment and convert it into direct current energy through conversion, storage, and other means, which can be used by electronic devices. This way is undoubtedly the greatest extent to reduce the waste of energy and greatly improve the energy's utilization, which has a decisive significance to solve the energy problem.

As we know, wearable electronic devices generally have the following two characteristics. Firstly, the energy demand is generally small. Secondly, its power supply equipment replacement is relatively complex, which means we have to face the problems to apply a power module that can work for a long time. With the development of technology, the wearable energy collection system can be divided into two directions. Firstly, the volume of energy acquisition systems will be reduced smaller and smaller to eventually integrate it into the energy modules in wearable electronic devices. Another one is to continuously optimize the energy collection system, design its own storage module, collect and store the environment energy, and unify the management.

A large number of scientific researchers are exploring the perfect combination of wearable and energy collection in those two ways mentioned above. Georgia Institute of Science and Technology, the Wang Zhonglin team from the Institute of Chinese Academy of Sciences, and the H. Alshareef research team from King Abdullah University

of Science and Technology (KAUST) have designed a bracelet that combines the energy collection and storage inside the device to provide sustainable energy for the wearable devices [1]. At the same time, Cheng Jianli, Wang Bin, and others from the Institute of Chemical Materials of China Engineering and Physics Institute have designed a fiber optic capacitor shown in Figure 1, which has 5.1% energy conversion efficiency and is of great significance to the energy supply for the wearable electronic equipment [2].

By looking for energy collection devices that are more efficient and applicable to the wearable electronic equipment, the Takao Someya team from Tokyo University and the Japan Institute of Physical Chemistry and Research has designed a superflexible organic solar cell that is 13% efficient in transferring energy, and the solar cells are still able to maintain a good device performance after multiple stretching tests [3]. Professors Pietro Cataldi and Mario Caironi from the Institute of Science and Technology in Italy have designed a planar flexible thermoelectric device with good flexibility and washing stability, which provides a profound meaning for the development of wearable thermoelectric devices [4]. Professor Yanliang Zhang from the University of Notre Dame Aerospace and Mechanical Engineering has designed a flexible thermoelectric acquisition unit through its improved 3D printing technology, which can show a high power density of 7.65 mw/cm^2 under the temperature gradient of 60 k, which is a great help for the application of thermoelectric collectors used in wearable products. A flexible 3D fabric was developed by Professor Zhi Chunyi from the City University of Hong Kong and Hu Hong from the Hong Kong Institute of Science and Technology, which can be able to provide energy to the electronic devices by friction. A yarn-based triboelectric nanogenerator for energy acquisition was prepared by Xiong Pu, Weiguo Hu, and Zhonglin Wang from the Beijing Institute of Nanoenergy and Systems, Chinese Academy of Sciences [5]. The research group of Professor Hu Chenguo from Chongqing University and Professor Guo Hengyuan from Beijing Institute of Nanoenergy and Nanosystems, Chinese Academy of Sciences, used traditional weaving techniques to produce self-charging energy fabrics for collecting human movement energy with the characteristics of mass production [6].

In energy storage of wearable electronic devices, the research team led by Associate Professor Chunyi Zhi of the City University of Hong Kong has built a set of evaluation standards for energy storage devices of wearable devices by analyzing the flexibility, tensile, and wearability of flexible energy storage devices [7], which provides a direction for the development of wearable energy memory to a certain extent. A flexible fiber membrane lithium-sulfur battery was designed by the research group of Professors Yan Wei and Yu Shujiang from Xi'an Jiaotong University and Xi Kai and Vasant Kumar from the University of Cambridge [8]. Jianli Cheng, Bin Wang from the Institute of Chemical Materials, CaEP, and Jun Lu from Argonne National Laboratory together designed a high flexibility fiber Li-CO2 battery [9]. Chen et al. from the Department of Materials, ETH Zurich, made a highly elastic thin-film cell [10]. A sodium ion battery with high conductivity, high mechanical strength, and high flexibility was prepared by Professor Junmin Yan's research group from Jilin University using industrial wastewater and waste cotton fabric [11]. The research team of Professor Geng Fengxia from Suzhou University prepared a high magnification flexible thin-film electrode battery by using two-dimensional materials [12] and so on.

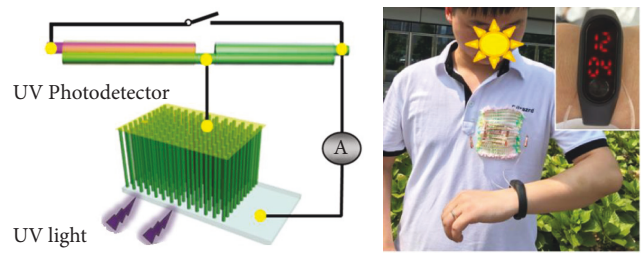

Figure 1: Fiber optic containers and energy collecting bracelets.

As RF energy collecting, it is found that researchers basically collect frequency bands around 1.8 GHz, 2.1 GHz, 2.3 GHz, 2.4 GHz, 2.5 GHz, 3.3 GHz, 3.8 GHz, 5.2 GHz, and 5.5 GHz (mainly WIFI frequency band and WIMAX frequency band). Meanwhile, the current research directions of researchers mainly include the following: (1) trying different flexible materials to prepare multiband antenna models; (2) trying to use metamaterial technology to improve the gain of RF energy collection antenna [13–17]. Although there is no flexible RF energy collector that is fully applicable and has reached the application level at present, as the attempt in literature, the flexible RF energy collector suitable for wearable devices will one day become a product and appear in people's life [18].

At present, conclusively, there are two ways in most researches on maximum power output algorithm of energy acquisition. First, add the DC-DC function after each energy acquisition module to increase the output voltage value and use some algorithm like MPPT (Maximum Power Point Tracking) to control the energy discharging [19]. Second, add only one DC-DC module after several energy modules and use the passive mode (only the energy module with the highest voltage value can discharge) to supply the energy power to load. The first method leads to a high loss of environmental energy in multiple DC-DC stages, reducing the utilization of hard-won environmental energy. For the second method, the discharging power of the energy module passively selected is not necessarily the maximum; that is to say, the energy module with the maximum discharging power cannot discharge, resulting in energy waste.

Based on the circuit topology of the second way (only one DC-DC module), this paper uses the power trajectory tracking algorithm to actively supply the energy power to load. Compared with passive discharge, the active discharge method can effectively improve the utilization of environmental energy.

This paper analyzes the architecture of mixed environment energy collection system, then, respectively, analyzes and establishes the models of thermoelectric collector and RF energy collector, and makes the physical objects of these two collectors at last in Section 2. It designs a heart rate

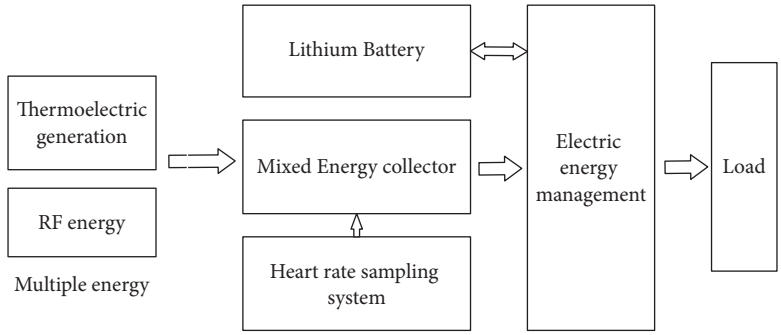

Figure 2: Wearable device environmental energy acquisition and management system.

sampling algorithm to accurately collect the required environmental energy voltage and current information in Section 3, establishes an energy management model with the maximum power output algorithm based on power trajectory tracking and simulates it in Section 4, and at last sets an experiment to verify the effect of this energy collection system in Section 5.

2. Analysis and Design of Mixed Energy Systerm

Contraposing the actual environment of human activities, the energy source of the wearable energy acquisition system includes heat energy (for the temperature difference between the human body and the environment) and radiofrequency energy (for the external environment of human beings).

Due to the uncertainty and weakness of environmental energy, we still use lithium battery as the main power supply of wearable devices and the two mixed energies as supplementary power.

It is well known that environmental energy can easily change according to environmental conditions. In the case of poor environmental conditions, the energy output is extremely weak, so it is needless to detect the port voltage of the environmental energy module. The port voltage has to be detected when the environmental conditions become better, or the energy module has stored enough output energy. Therefore, this paper adds a heart rate sampling system for the environmental energy module to avoid invalid real-time voltage or current detection and accurately collect the port voltage value on the premise of saving energy.

To effectively improve the utilization rate of environmental energy, this paper designs a mixed energy collector. The energy collector will control the sampling sequence of the heart rate sampling system and control the environment energy supplied to the load or charging the battery efficiently. The block diagram of wearable environmental energy collection system designed in this paper is shown in Figure 2.

2.1. Thermoelectric Energy Collection. The basic principle of thermoelectric energy collector is the same as that of thermoelectric power generation, which is to connect two kinds of semiconductor thermoelectric materials, *N*-type and *P*-type, in series with the conductive plate with good thermal conductivity and conductivity and then fix them on

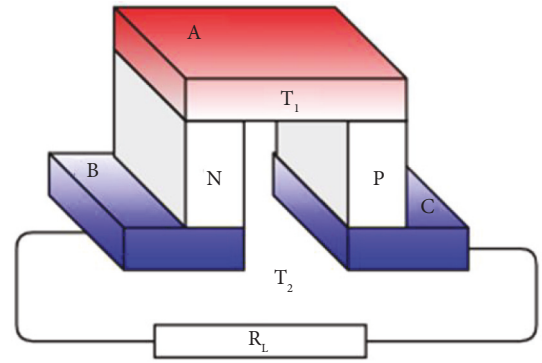

Figure 3: Structure drawing of monomer thermogenerator.

the ceramic plate with good thermal conductivity, and then it can get the thermoelectric power generation or thermoelectric energy collection.

In practical application, the hot side of the thermoelectric material slice is closely connected with the heat source, and the temperature of the cold side is reduced as far as possible by means of heat dissipation so that the temperature difference is formed on both sides of the device. According to the Seebeck effect, a voltage will be generated in the loop, and a current will flow through the load. In order to achieve the required power, usually in practical applications, 18–128 groups of monomers are arranged in series or parallel to form thermoelectric devices.

2.1.1. Thermoelectric Model Analysis. Thermoelectric devices will be evaluated using the following parameters to design and implement efficient hardware thermoelectric systems.

(1) Output Power of Thermocouple. As shown in Figure 3, the thermocouple arrangement structure is generally adopted in the basic units of thermoelectric power generation elements. According to the Seebeck effect, when the temperature at both sides of the element is T_1, T_2, and $T_1 > T_2$, the voltage in the loop is [20, 21]

$$U = \alpha(T_1 - T_2). \tag{1}$$

Due to the internal resistance r of the thermoelectric element itself, only part of the voltage generated by the thermoelectric element is loaded onto the load resistance R_L. That is, the voltage presented on the load resistance (R_L) at this time is the actual output voltage of the thermoelectric device, which is usually expressed as

$$V_{\text{out}} = \alpha(T_1 - T_2)\frac{R_L}{R_L + r} = \frac{m\alpha(T_1 - T_2)}{1 + m}. \tag{2}$$

In the above formula, the ratio of load resistance to internal resistance is expressed as m. Furthermore, the loop current can be expressed by the following formula:

$$I = \alpha\frac{(T_1 - T_2)}{R_L + r}. \tag{3}$$

Through the above expressions of voltage and current, the output power of the temperature difference generator can be calculated as follows:

$$P = \frac{\alpha^2(T_1 - T_2)^2 R_L}{(R_L + r)^2} = \frac{m}{(1 + m)^2}\cdot\frac{\alpha^2(T_1 - T_2)^2}{r}. \tag{4}$$

When $m = R_L/r = 1$, that is, when the load resistance value is equal to the internal resistance value of the thermoelectric element, its output power is the maximum, and the maximum value is [22]

$$P_{\max=}\frac{\alpha^2(T_1 - T_2)^2}{4r} = \frac{\alpha^2\Delta T^2}{4r}. \tag{5}$$

(2) Power Generation Efficiency of Thermoelectric Generator. In order to investigate the power generation efficiency of thermoelectric elements, the total heat Q_h absorbed from the heat source needs to be considered first. Q_h is composed of joule heat, heat conduction, and Partie heat, which can be expressed as

$$Q_h = \alpha T_1 I - \frac{1}{2}I^2 r + \lambda(T_1 - T_2), \tag{6}$$

where λ is the thermal conductivity of thermocouple material and Seebeck coefficient between α and two materials (P- and N-type semiconductor) can be expressed as follows:

$$\alpha = \alpha_P - \alpha_N. \tag{7}$$

Thus, the power generation efficiency of thermoelectric generator can be obtained:

$$\eta = \frac{P_0}{Q_h} = \frac{\alpha^2(T_2 - T_1)^2 R_L/(R_L + r)^2}{\alpha T_2 I - (1/2)I^2 r + \lambda(T_2 - T_1)}. \tag{8}$$

Arrange it again:

$$\eta = \left(\frac{T_2 - T_1}{T_2}\right)\left[\frac{m}{(1 + m) - (T_2 - T_1/T_2) + (1 + m)^2/ZT_2}\right], \tag{9}$$

where Z is the optimal value coefficient of the material, $Z = \alpha^2/RK$.

When $d_\eta/d_m = 0$, which also is $m = (1 + Z\overline{T})^{1/2}$, the output efficiency of the thermoelectric generator is the highest, where $\overline{T}$ represents the average temperature between the cold side and the hot side of the thermoelectric element; namely,

$$\overline{T} = \frac{(T_2 + T_1)}{2}. \tag{10}$$

Thus, the maximum efficiency can be expressed as follows:

$$\eta_{\max} = \frac{T_2 - T_1}{T_2}\cdot\frac{\sqrt{(1 + Z\overline{T})} - 1}{\sqrt{(1 + Z\overline{T})} + T_1/T_2}. \tag{11}$$

2.1.2. Thermoelectric Module Design. According to previous studies, the circuit model of thermoelectric module is shown in Figure 4:

$$R_{TEG} = \frac{R_{TE} + R_S}{R_{TE}\cdot R_S}. \tag{12}$$

Then, the basic relationship can be obtained from the above model:

$$\Delta T_{TEG} = \frac{R_{TEG}}{R_{thA} + R_{thB} + R_{TEG}}.\Delta T. \tag{13}$$

From the above analysis, it can be seen that the difference between human body temperature and ambient temperature (ΔT) is obviously larger than the difference between the cold side and hot side (ΔT_{TEG}) of the thermoelectric element (*TEG* element); that is, the actual temperature difference (ΔT_{TEG}) between the two sides of the thermoelectric device is relatively small. Meanwhile, the parallel structure of multiple thermocouples inside *TEG* makes its thermal resistance smaller [23–26]. As a result, the temperature difference in the environment is much greater than the temperature difference applied to the thermoelectric element. However, it should also be noted that some phenomena in the external environment (such as air flow) can make the heat exchange on the *TEG* surface more active because thermal resistance R_{thA} is affected by thermal radiation and thermal convection between the thermoelectric element and the external environment; that is, when wind flows on the surface of *TEG* in the environment, its value will be greatly reduced. Therefore, the performance of *TEG* is closely related to the external environment.

To explore the performance of thermoelectric elements more definitively, we can make the following assumptions. Assuming that the number of thermocouples contained in *TEG* is N, the Seebeck coefficient of thermoelectric materials is α, the temperature difference between the two surfaces of *TEG* is ΔT_{TEG}, and the voltage generated by *TEG* is V_T; the following relation can be obtained:

$$V_T = N\cdot\alpha\cdot\Delta T_{TEG}. \tag{14}$$

A simplified electrical model is constructed with *TEG* components as the source, and its basic style is shown in Figure 5. *TEG* is equivalent to a series of voltage source V_T and

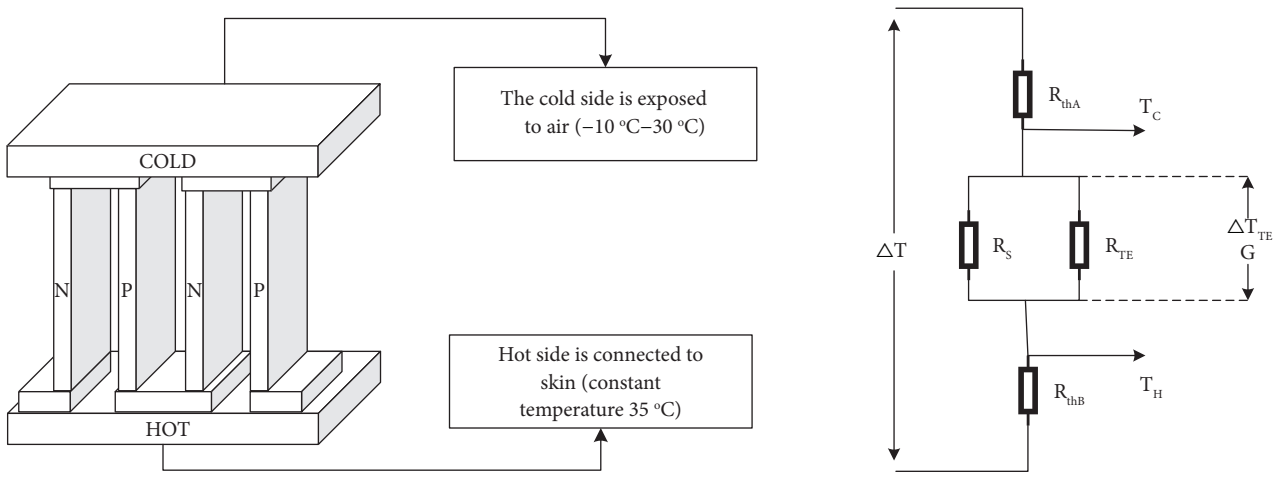

Figure 4: *TEG* model and electrical model based on human body.

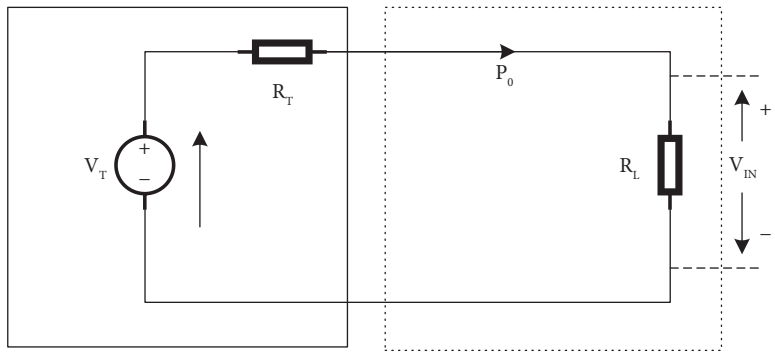

Figure 5: Equivalent electrical model of *TEG*.

internal resistance R_T, and the external circuit is replaced by resistance R_L. Meanwhile, the value of the output power P_O of the thermoelectric element depends on its internal equivalent resistance R_T and the resistance R_L of the external load circuit. Based on basic circuit principles, the output power P_O of a thermoelectric element can be expressed as follows:

$$P_O = \frac{V_T^2}{(R_L + R_T)^2} \cdot R_L. \tag{15}$$

According to the basic properties of the above equation, the power curve of *TEG* can be basically expressed as a quadratic function. When the external resistance R_L is equal to the internal resistance R_T of the *TEG* element, the maximum power point can be obtained, which could be expressed as

$$P_O = P_M = \frac{V_T^2}{4R_T}. \tag{16}$$

2.1.3. Thermoelectric Module Design. There are many factors that affect the performance of thermoelectric acquisition devices. To select suitable thermoelectric devices, it is necessary to comprehensively analyze the advantages of thermoelectric materials, the shape of thermocouple arms, and the structure of thermoelectric devices.

In order to build thermoelectric devices with better performance, *N*-type and *P*-type materials can be added to semiconductor materials to make them have similar advantages. Such processing technology is also relatively simple and easy to implement. At the same time, the physical size (geometric size) of thermocouple also affects the energy conversion efficiency of thermoelectric devices. In general, when the two materials of the galvanic arm have different optimal values, their geometric dimensions are usually different.

In this paper, thermoelectric devices with conventional longitudinal structure are selected. To closely combine wearable characteristics with its structure, 3D printing technology is used to design the structure as shown in Figure 6(a). Through reasonable placement, the thermoelectric generator perfectly reflects the wearable characteristics. Figure 6 shows a thermoelectric generator connecting to the mixed energy collector designed in this paper.

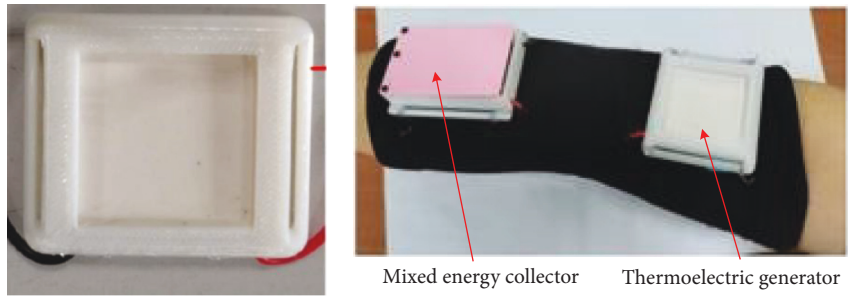

(a) (b)

Figure 6: Thermoelectric collection module: (a) 3D shell and (b) connection of thermoelectric generator and mixed energy collector.

2.2. RF Energy Collection

2.2.1. Analysis of RF Energy Collection Model. RF energy collection can avoid the influence of harsh environment and light and is more stable than solar energy and wind energy.

Since the RF energy used in this paper belongs to the energy that exists in the environment and may be transmitted by multiple signal sources with uncertain transmission power, the RF energy collector shall consist of at least two parts, a receiving antenna and a filter rectifier circuit. Receiving antenna is the first device to receive RF energy from space to the circuit, and its performance determines the effect of RF energy collector. The parameters of the receiving antenna are resonance frequency, bandwidth, return loss, receiving efficiency, and so on. The larger the harmonic frequency bandwidth is, the more environmental RF energy can be received, and the higher the efficiency of the receiving antenna is, the higher the efficiency of receiving RF energy is.

For RF energy receiving antenna models in space, we usually have Free Space model, Dual Ray Ground model, and Rayleigh model.

(1) Free Space Model. According to the Friis equation, the power that an energy receiver can receive is

$$P_R = \frac{P_T G_T G_R \lambda^2}{(4\pi\ d)^2 L}, \tag{17}$$

where P_T is the transmitting power of the transmitter, G_T is the transmitting antenna gain of the transmitter, G_R is the receiving antenna gain of the energy receiver, λ is the wavelength of RF signal, and d is the distance between the transmitting antenna and the receiving antenna.

(2) Dual Ray Ground Mode. As RF signals reach the receiving antenna through a direct path and a reflected path, respectively, the power obtained by the energy collection antenna from the energy transmitter is as follows:

$$P_R = P_T G_T G_R \frac{h_t^2 h_r^2}{d^4}, \tag{18}$$

where P_T is the transmitting power of the transmitter, G_T is the transmitting antenna gain of the transmitter, G_R is the receiving antenna gain of the energy receiver, h_t is the height of the transmitting antenna, h_r is the height of the receiving antenna, and d is the distance between the transmitting antenna and receiving antenna.

Table 1: Radiofrequency signal bands in the environment.

Mobile operators	Frequency band (MHz)	Tower signal (G)
China Mobile (TD-LTE)	2320–2370	4
China Unicom (TD-LTE)	2300–2320	4
China Telecom (CDMA2000)	2110–2125	3

(3) Rayleigh Model. Rayleigh model stipulates that the received power obtained by the energy collection antenna from energy transmitters is (the power that relay nodes/secondary users can receive from RF signals transmitted from source nodes/primary users)

$$P_R = P_R^{\text{det}} \times 10^L \times \log(1 - \text{unif}(0,1)), \tag{19}$$

where $L = -\alpha \log 10(d/d_0)$ is the path loss factor of the radio channel, d_0 is the reference distance, P_R^{det} is the accepted power calculated by a deterministic model, and unif $(0, 1)$ is the random number generated between 0 and 1.

In the assumption of this paper, the radiofrequency energy in space is radiated by multiple energy sources. The power of the radiation energy source and radiation direction and the distance between the radiation antenna and the receiving antenna are uncertain. Therefore, the Rayleigh model is more consistent with the actual situation in this paper.

We use the Rayleigh model as a reference for modeling and analysis, which can better simulate the characteristics of RF energy in this paper.

2.2.2. Design of RF Energy Collection Module. RF energy collector usually consists of three parts: a receiving antenna, a rectifier, and a voltage doubling circuit. The collector needs to be measured by working bandwidth, return loss, efficiency, gain, and input impedance. Combined with the measurement standards and based on the actual application scenarios, this paper will design an energy collection antenna that can collect RF energy in the environment and is suitable for wearable.

Table 2: Basic parameters of a receiving antenna.

Parameters	Parameters range	
Working frequency range	2.1 GHz (2.1–2.125 GHz)	2.3 GHz (2.3–2.37 GHz)
Return loss	2.1 GHz (−10 dB)	2.3 GHz (−10 dB)
Gain	2.1 GHz (1.50 dB)	2.3 GHz (3.0 dB)
Impedance characteristic	(40–60) + (−10–10) j	

Figure 7: Antenna basic shape diagram: (a) front side and (b) back side.

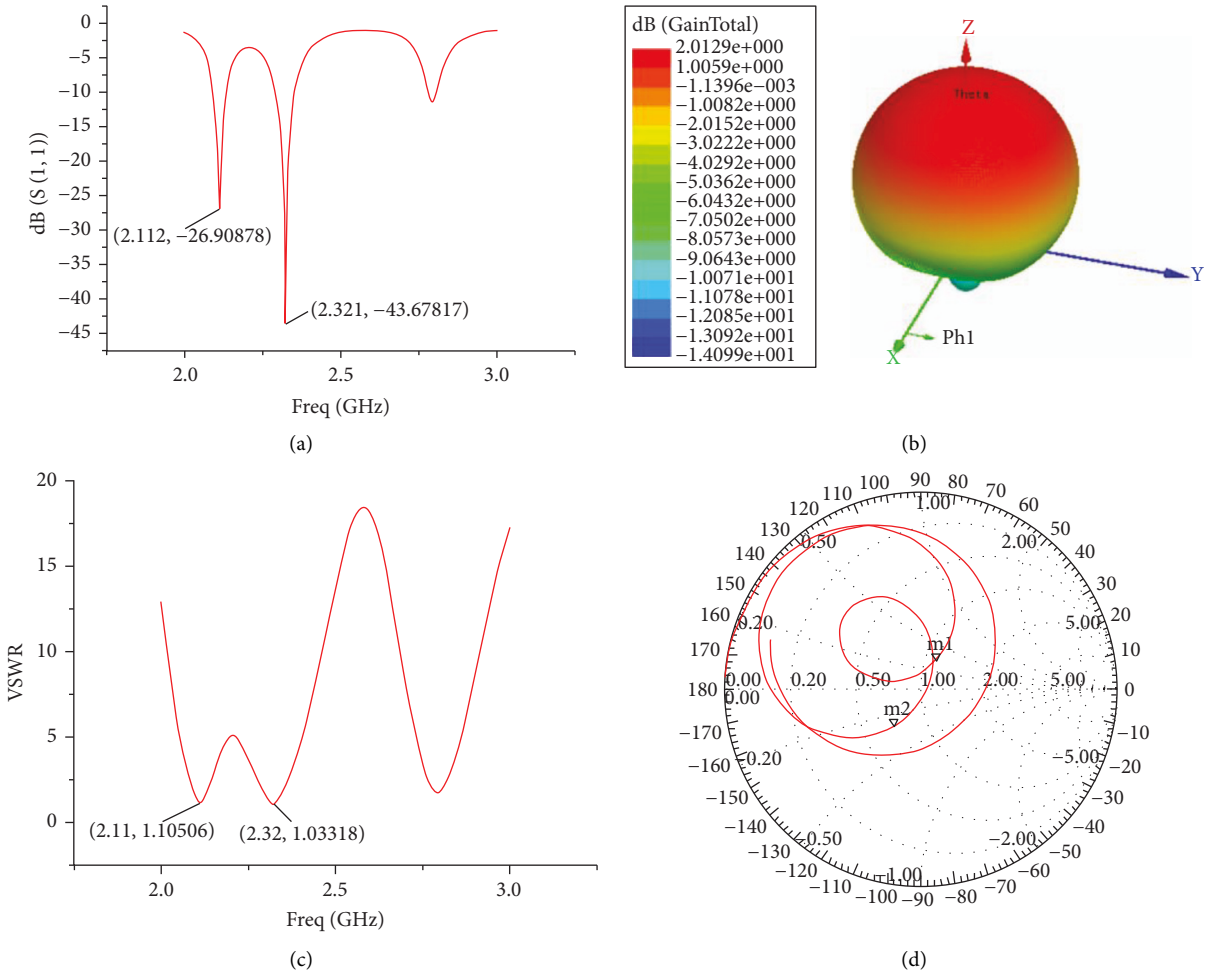

Figure 8: Antenna simulation results: (a) antenna return loss, (b) antenna radiation patterns, (c) antenna standing wave ratio, and (d) Smith chart.

For the selection of frequency band, considering the frequency band of the signal transmission tower of China mobile operators, which is shown in Table 1, the 3G (near 2.1 GHz) and 4G (near 2.3 GHz) signals in the environment are taken as the final target frequency band for collection.

Normally, the return loss S11 and gain value are more important in the antenna index. Therefore, the antenna designed in this paper has basically defined the above parameters, and the specific requirements are shown in Table 2.

The basic structure of the antenna is designed by HFSS software in this paper. Firstly, the basic size of the antenna is calculated according to the plate medium coefficient and antenna formula. Secondly, in order to get a broadband antenna, a slot is needed on the back of the antenna. Finally, to save the cost, this paper uses the common RF4 plate to design and simulate the antenna.

With the help of 3D electromagnetic simulation software HFSS, according to the conventional calculation formula of microstrip antenna size, L slot's characteristics on the back, FR4 plate parameters, the expected antenna operating frequency, and so on, the antenna structure is designed as shown in Figure 7.

After a long time of calculation with HFSS, the antenna's S11 return loss, radiation patterns, standing wave ratio, and Smith chart are obtained as shown in Figure 8.

From Figure 8(a), we can see that it has a good return loss of S11 at frequencies 2.1 GHz and 2.3 GHz. The antenna standing wave ratio is very closely equal to 1 at 2.1 GHz and 2.3 GHz, which is shown in Figure 8(c). And the Smith chart in Figure 8(d) represents the impedance characteristics of antenna. The antenna in this paper is linearly polarized because there is only pole at "$m1$."

The antenna layout is slightly arranged in the software Altium Designer for processing, and the physical antenna made of FR4 plate is shown in Figure 9.

The high-frequency AC energy received by RF antennas cannot be supplied directly to electronic devices. That means it is necessary to design a reasonable rectifier circuit matching the antenna to convert the high-frequency electromagnetic energy into DC energy (RF-DC), which can ultimately be provided to the electronic equipment load. The process is shown in Figure 10. RF receiving antenna and rectifying circuit are collectively called RF energy rectifying antenna.

The rectifier circuit is the core component of the rectifier antenna, which is generally divided into series type, parallel type, single-stage voltage doubling type, Greinacher type, and bridge rectifier type according to its way to access a circuit. Through analyzing and comparing the above structures, it is found that the overall effect of half-wave rectification is better than full-wave rectification when the input power is low. Therefore, this paper designed a first-order voltage doubling rectifier circuit using the half-wave rectification, which is suitable for RF energy collection antenna.

Using HFSS software to design the impedance matching circuit, input filter part, rectifier part, and output filter and then optimizing the rectifier circuit according to the desired rectification efficiency and rectification voltage, this paper got a voltage doubling rectifying circuit model shown in Figure 11. After making the rectifier circuit with FR4 plate, we connect the antenna and rectifier circuit together through the coaxial line, which is shown in Figure 12.

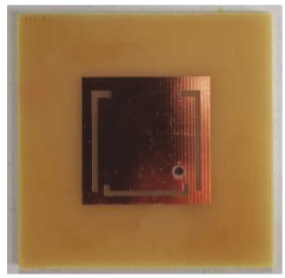

Figure 9: Physical antenna made of FR4 plate.

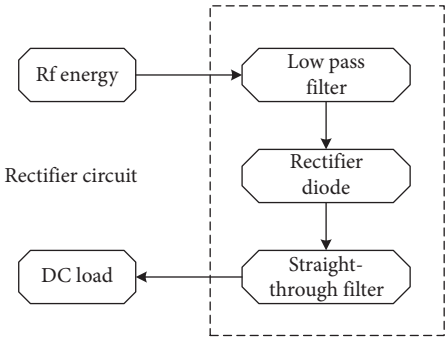

Figure 10: Basic diagram for RF-DC.

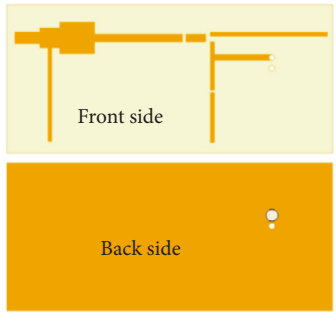

Figure 11: Voltage doubling rectifying circuit model.

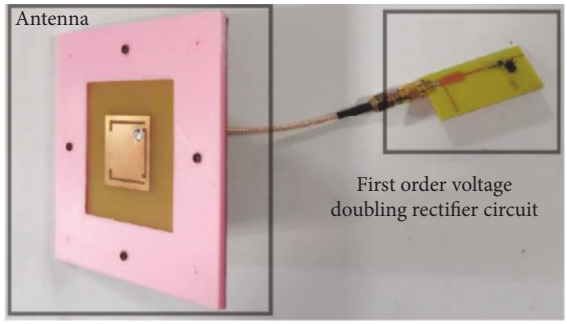

Figure 12: Material object of rectifying antenna.

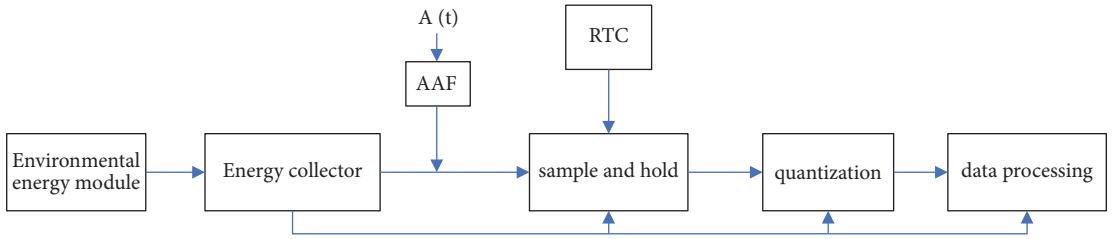

Figure 13: Structural diagram of heart rate sampling system.

3. Heart Rate Sampling System

Environmental energy is characterized by instability and weakness. When an energy module is in an unfriendly environment, it is very likely that the module will not be output. If the port voltage of each energy module is collected in real time without judgment, the additional system power consumption will be increased.

Therefore, according to the characteristics of environmental energy, this paper designed a heart rate sampling system driven by an environmental energy module. The sampling sequence obtained by the system can be approximated to a nonuniform sampling sequence, which is analyzed by combining the theory of nonuniform sampling and restored by the nonuniform sampling reconstruction method.

The heart rate sampling system based on environmental energy collection is shown in Figure 13. As the controller of the system, the energy collector also needs to control the heart rate sampling system, while the sampling system is controlled by the output voltage of the environmental energy module.

$A(t)$ is the sampled signal. The discontinuous energy generated by the environmental energy drives the sampling device to perform the sampling work; at the same time, the sampling sequence is thus obtained. The discontinuous energy replaces the continuous energy supply in the existing traditional sampling system to finish the original signal's sampling.

The RTC is used to record the time of the sampling site, and its primary responsibility is to provide an accurate time baseline.

Due to the instability of environmental energy, the sampling system is prone to power failure. Therefore, a low-power power failure storage system "sample and hold" is designed in this paper.

4. Energy Management Model and Simulation

In most environmental energy collection circuit topologies, a DC-DC is configured for each energy collection module, which greatly increases the overall energy consumption of the system and reduces the energy utilization efficiency. The traditional environmental energy collection circuit is shown in Figure 14.

Therefore, this paper designs an energy collection and management module with only one DC-DC and only one environmental energy output at the same time. In order to ensure the maximum environmental energy will be output,

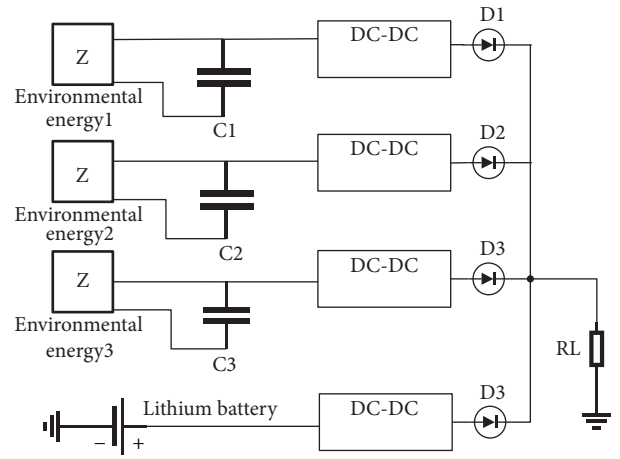

Figure 14: Traditional environmental energy collection circuit diagram.

we should know which one is maximum, which means we should establish a dynamic model of load to confirm the maximum energy at every "current time" [27].

This paper presents an energy management circuit topology and its algorithm, which is called power trajectory tracking for the first time. Its circuit topology is shown in Figure 15.

It can be seen that there is only one DC-DC module in this circuit topology, and all energy sources (except batteries) use the same DC-DC, which can effectively reduce the loss of environmental energy in the conversion process. However, the problem caused by this topology is that energy sources with different port voltages cannot output their energy at the same time. Only one energy can be output at a time, and other energies are temporarily stored by the ultracapacitors.

During the operation of this circuit, two (or more) energies may complete storing and need to discharge to the load or to the battery. According to previous studies, the order of energy release is generally determined according to the current voltage of the energy module; that is, the one with the highest voltage is the first to discharge. However, due to the randomness of environmental energy and the functional difference of different energy modules, the power released by the energy module with a high voltage value is not necessarily the maximum (the discharge current needs to be considered).

Assume that the voltage and discharging power per unit time of two energy modules are V1 and V2 and P1 and P2,

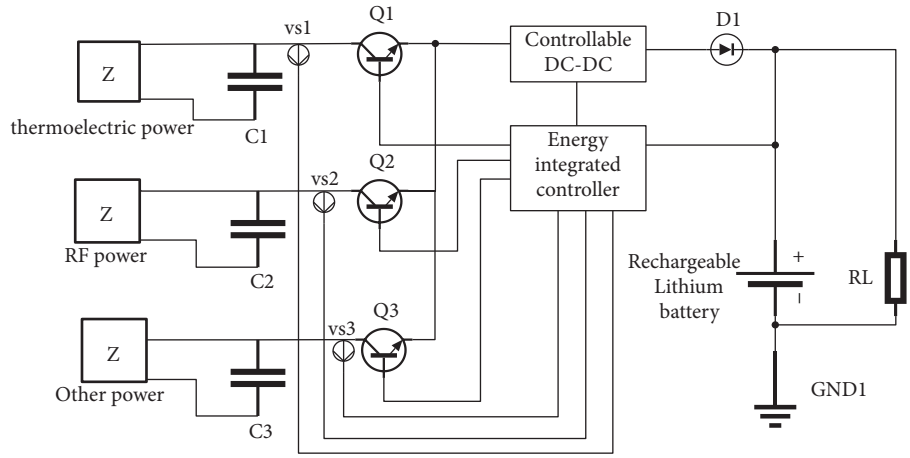

Figure 15: Energy management circuit topology. C1, C2, and C3 are ultracapacitors, VS1, VS2, and VS3 are voltage sensors of the heart rate sampling system, Q1, Q2, and Q3 are three controllable audions, and D1 is a single guided diode.

respectively. Even V1 > V2, but P2 > P1 may occur. In view of this situation, in order to effectively improve the energy utilization, the maximum power control strategy based on power trajectory tracking is proposed for the first time in this paper.

The maximum power control strategy based on power trajectory tracking is to control the discharge sequence of the energy module in a sufficiently small period to ensure the environmental energy discharge with the maximum power output capacity at the moment, that is, to ensure the maximum energy obtained by the load at the moment. Based on this, the flow diagram of this energy management system is designed as shown in Figure 16.

To effectively improve the efficiency of DC-DC, this paper sets a voltage threshold, and only the energy module that meets the threshold is allowed to output electric energy.

In order to ensure that the energy module with the highest power discharges at any time, we must know the discharge capacity of all energy modules. Therefore, we need to measure the discharge power of all energy modules in different environments, synthesize the power curve and save them, and form a large database of power curves at last.

This means that we need to track the power curve in the current environment, similar to the trajectory tracking strategy of robotic devices [28–30].

In a real system, how to define different environments is an issue to consider. After studying enough environmental energy collection modules, it is found that the port voltage of the energy module has a certain proportional relationship with the external environment. Therefore, the control strategy in this paper stipulates that those different environmental energies are determined by different energy module port voltages.

Therefore, the above description can be summarized as follows: we need to measure the discharge power of all energy modules under different initial voltages, form and save power curves under different initial voltages, and form a large database of power curves under different initial port voltages.

The procedure power track tracking of all power modules that meet the voltage threshold is as follows:

(1) Measure the port voltage of all energy modules by the heart rate sampling system and open the energy modules meeting the voltage threshold 100 times in turn to obtain 100 power points of different energy modules.

(2) Fit the measured power points into P-t curves using genetic algorithm.

(3) Select a small unit time, calculate the power integral value in unit time according to this curve, save this power integral value, and form a large database of power integral values in unit time under different energy modules and different voltage values.

Next, we will choose the power module with the maximum power integral value at the current time to discharge to the load. During the discharge process, check whether the voltage of each energy module has a voltage mutation or whether the terminal voltage of the new energy module meets the voltage threshold. If no, perform the previous discharge sequence. If yes, check whether the power curve of the energy module at the current voltage is stored in the power curve database. If not, it is necessary to collect the power values of 100 energy modules that meet the requirements again and fit them into P-t curves, integrate them again, and save and update the large database again. However, if the data exists in the database, the energy module to discharge at the next moment can be determined directly according to the integral value of power per unit time saved in the big data.

The power integral large database saves the power integral values of different energy modules in a microperiod under certain environmental conditions. Any change in the output power of an energy module due to environmental changes will be measured again and saved. That is, the database can self-update, self-preserve, and self-learn according to the measurement system and according to the learning results to determine the discharge sequence of energy modules. The above process shows that the longer the system runs, the larger its database will be, but the more efficient its execution will be.

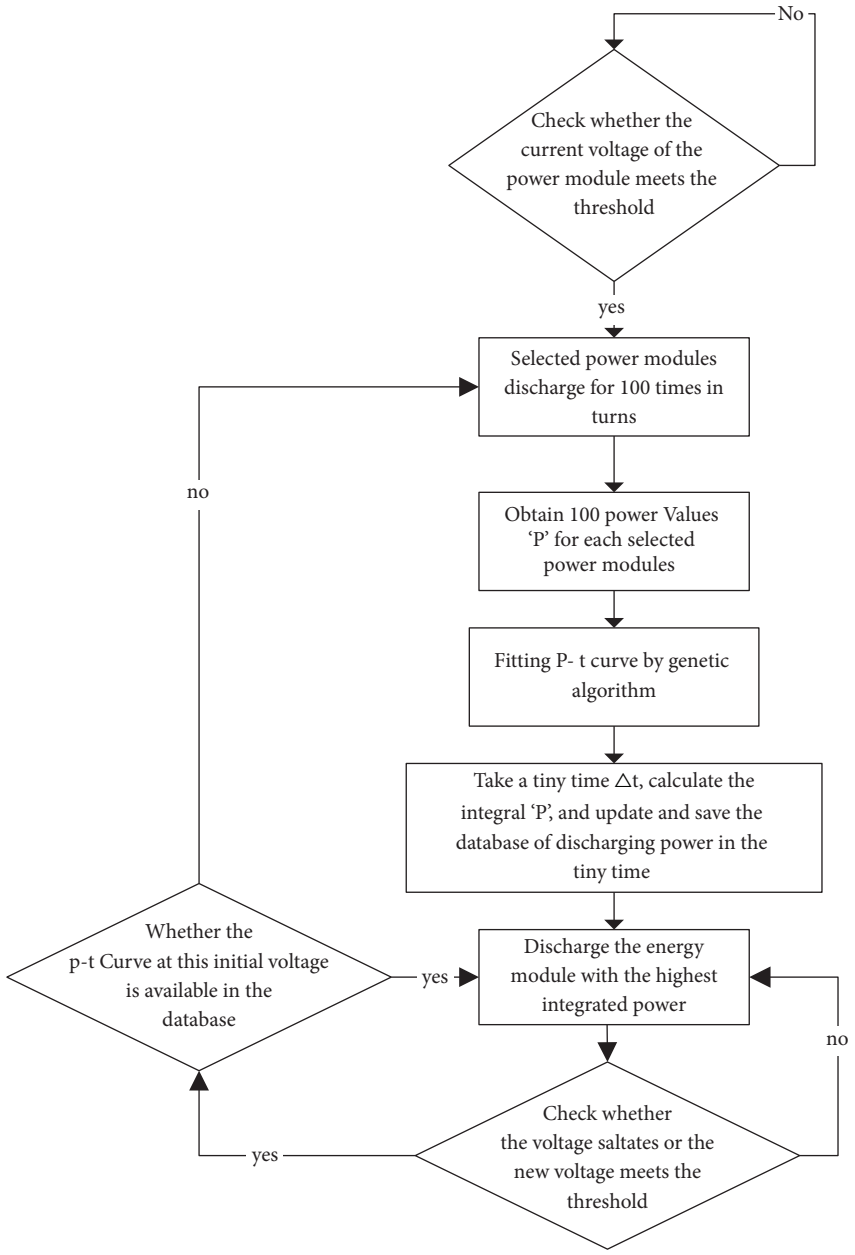

Figure 16: Flow diagram of maximum power control strategy based on power trajectory tracking.

The database does not use the original discharge power curve of the energy module (which can be obtained from the factory manual of the energy acquisition module) but uses the power curve synthesized by the real-time measuring system as a reference, which effectively avoids the error between the original power curve and the actual power curve caused by the decrease of the hardware working efficiency.

To sum up, the system can always maintain the maximum power output, effectively improve the utilization of environmental mixed energy, and improve the endurance of wearable devices.

In order to verify the effectiveness of the algorithm, a mixed environmental energy collection and management system model was established in Simulink, as shown in Figure 17.

Models ① and ② are RF energy collection and thermoelectric energy collection as clearly shown in Figures 18(a) and 18(b). To increase the output power of the thermoelectric collector, the temperature of the hot side is assumed to be 329 degrees Fahrenheit, and the cold side temperature is varied by the following formula:

$$Tc = \left(0.5 * t.^{(1/8)} + 1\right). * \cos\left(0.5 * t\right) + 325, \tag{20}$$

where Tc is the cold side temperature.

Model ③ is the mixed energy collection controller within the heart rate sampling system algorithm and the maximum power control algorithm based on power trajectory tracking.

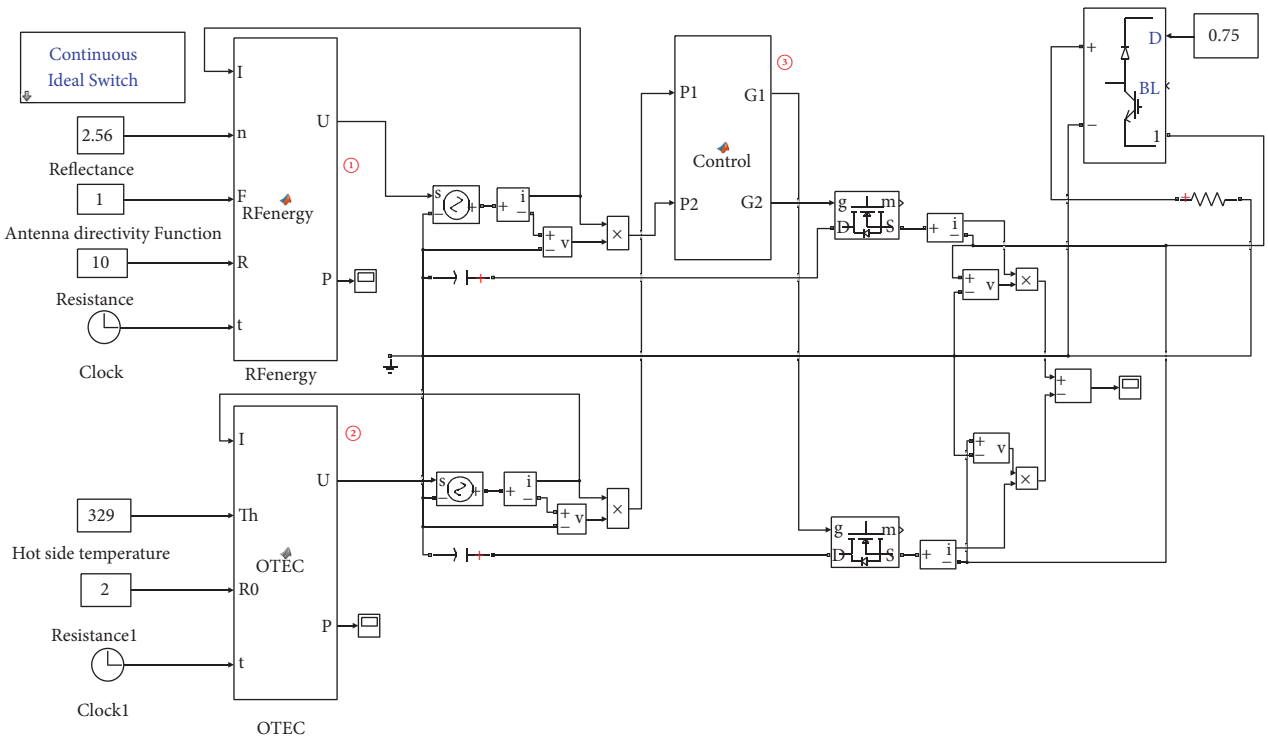

Figure 17: Mixed environmental energy collection and management system model.

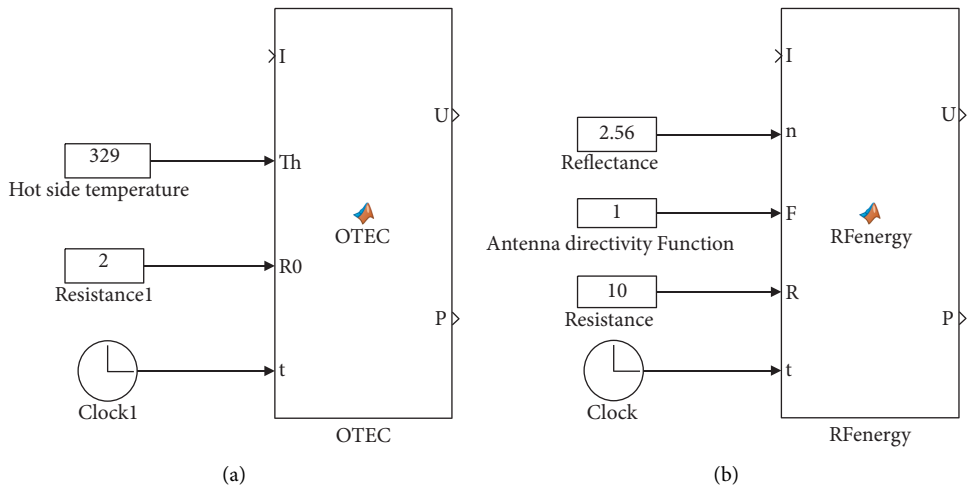

Figure 18: Thermoelectric and RF energy modules established in Simulink: (a) thermoelectric module and (b) RF energy module.

In the experiment, the RF energy module will collect the radiation energy from a router. Assume that the radiated power of the router changes to 1 W–3 W (randomly) and the RF energy collection circuit is placed in the far-field area of the router with a distance of 10 cm.

The output power curve was obtained as shown in Figures 19(a) and 19(b), under the condition of fixed load and randomly input within the preset interval.

According to the assumed power output curves of the two environmental energy modules, combined with the circuit topology and maximum power control strategy based on power trajectory tracking of this paper, the MATLAB simulation results are shown in Figure 20.

In Figure 20, we can see that the output power curve of the system is similar to Sine. Its highest point was 8.2 W (appeared at $t = 6.3$ s), and its lowest point was 4 W (appeared at $t = 12.8$ s). The sum of the two inputs in Figure 19 is 8.4 W when $t = 6.3$ s and 4.15 W when $t = 12.8$ s. By comparing the two sets of data, it is proved that the energy utilization ratio of the circuit topology combined with the maximum power algorithm is 97% at the maximum power and 96% at the minimum power. The simulation results show that the maximum power algorithm can keep high environmental energy utilization of the system.

The unreleased energy in the system is stored in the ultracapacitors and released only after the maximum power

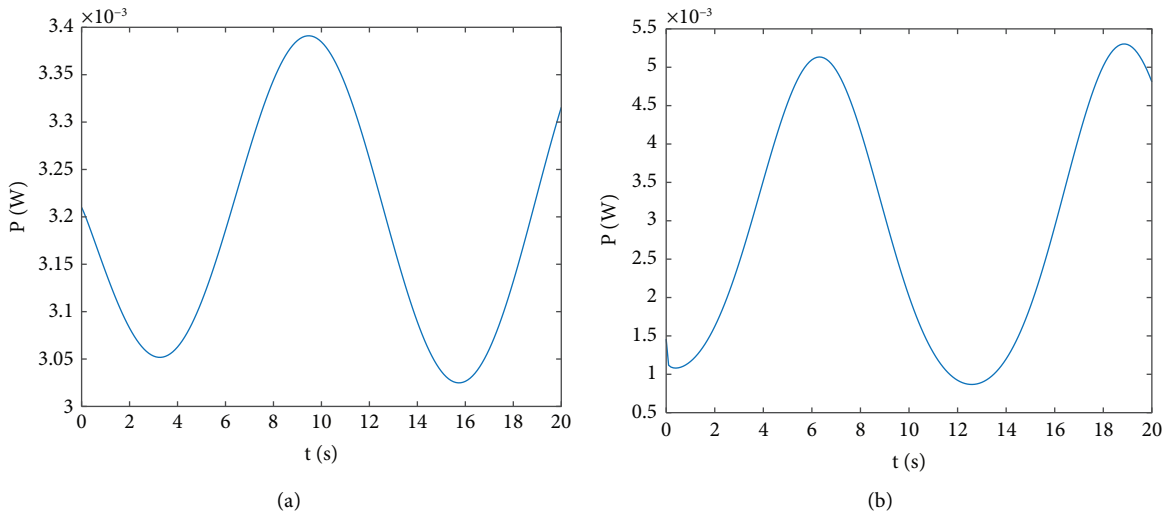

Figure 19: Simulated output power in MATLAB: (a) output power of RF energy module and (b) output power of thermoelectric module.

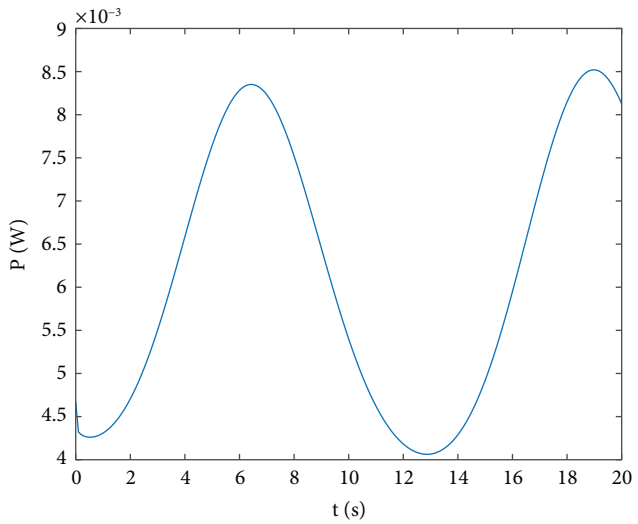

Figure 20: Simulated cure of maximum power control strategy based on power trajectory tracking.

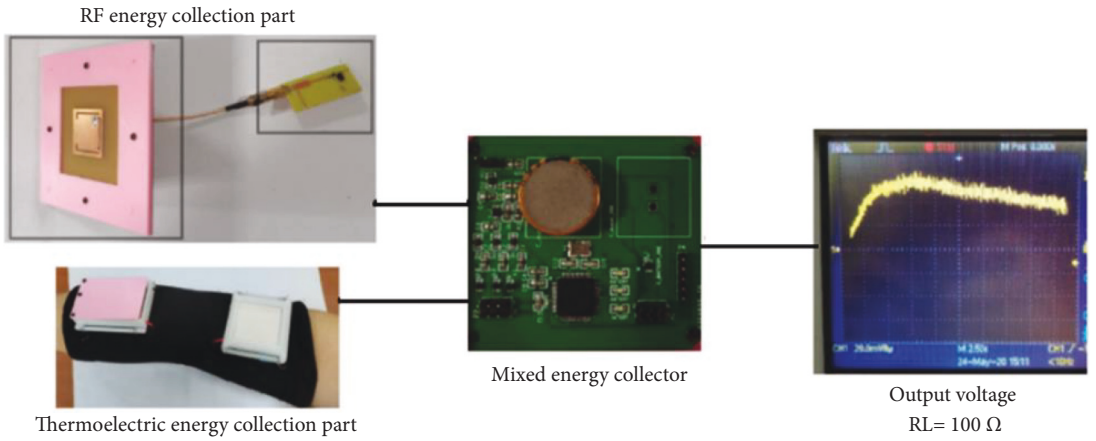

Figure 21: Test wiring diagram and output results.

Table 3: Power measurement on load.

Power	Time					
	0 s	1 s	2 s	3 s	4 s	5 s
Power of thermoelectric energy	0.11 mw	0.32 mw	0.49 mw	0.52 mw	0.48 mw	0.46 mw
Power of RF energy	0.29 mw	0.3 mw	0.31 mw	0.28 mw	0.29 mw	0.28 mw
Power of mixed energy (power of load)	0.39 mw	0.59 mw	0.77 mw	0.79 mw	0.72 mw	0.72 mw

condition is met. The smaller the minimum time Δt in the system is, the better the system control effect is. However, calculating the integral under too small Δt will occupy a lot of computing resources and increase the energy consumption of the system. Therefore, $\Delta t = 0.1$ ms is adopted in this paper.

5. Experimental Tests

In this paper, a real mixed energy control circuit is designed according to the circuit topology in the figure, using 100 Ω resistance as the load. In order to accurately verify the output effect of environmental energy, lithium batteries were not used in this experiment.

After testing the output curve of a single energy module, try to keep the environmental conditions unchanged (according to the theory of air flow rate and heat transfer, air flow has a great impact on the thermoelectric module, so it is difficult to ensure the condition's consistency).

We use the oscilloscope to observe the power curve on the load and set the oscilloscope time axis (horizontal axis) to 0.5 s one grid. The test result is shown in Figure 21.

In an effort to keep the environmental conditions of the single module measurement and the system measurement constant, the output power measured on the load is shown in Table 3.

There will be a measurement error due to measurement accuracy, environmental conditions, and so on. As shown in Table 3, the mixed energy management system ensures the high efficiency of environmental energy output through the method of maximum power control strategy based on power trajectory tracking.

6. Conclusions

In this paper, the model of thermoelectric collector and RF energy collector and the management model of two kinds of mixed energy are established by MATLAB. The discharge sequence of two kinds of energy modules is controlled by heart rate acquisition algorithm and power trajectory tracking algorithm. Simulink is used to simulate the above-mixed energy management model and maximum power trajectory tracking algorithm. Based on the simulation results, a mixed energy collection and management system is designed, and the effectiveness of the maximum power trajectory tracking algorithm is verified by experiments.

In the following research process, this paper will set more rigorous environmental conditions, use more environmental energy modules of different power levels, optimize control strategies, optimize experimental testing methods, and so on in order to achieve a better maximum power output effect of environmental energy.

Data Availability

All data included in this study are available upon request by contact with the corresponding author.

Conflicts of Interest

The authors declare that there are no conflicts of interest regarding the publication of this paper.

Acknowledgments

This work was supported by the National Natural Science Foundation of China (61803285 and 62001332) and the National Defense Pre-Research Foundation of China (H04W201018).

References

[1] M. He, Y.-J. Lin, C.-M. Chiu et al., "A flexible photo-thermoelectric nanogenerator based on MoS_2/PU photothermal layer for nfrared light harvesting," *Nano Energy*, vol. 49, 2018.

[2] P. Cataldi, M. Cassinelli, A. José et al., "Green biocomposites for thermoelectric wearable applications," *Advanced Functional Materials*, 2019.

[3] C. Dun, W. Kuang, N. Kempf, M. Saeidi-Javash, D. J. Singh, and Y. Zhang, "3D printing of solution-processable 2D nanoplates and 1D nanorods for flexible thermoelectrics with ultrahigh power factor at low-medium temperatures," *Advanced Science*, vol. 6, no. 23, Article ID 1901788, 2019.

[4] Z. Wang, Z. Ruan, W. S. Ng et al., "Integrating a triboelectric nanogenerator and a zinc-ion battery on a designed flexible 3D spacer fabric," *Small Methods*, vol. 2, no. 10, 2018.

[5] Z. Ren, Z. Qiao, H. Wang et al., "Wearable and self-cleaning hybrid energy harvesting system based on micro/nano-structured haze film," *Nano Energy*, vol. 67, Article ID 104243, 2019.

[6] J. Qi, A. C. Wang, W. Yang et al., "Hydrogel-based hierarchically wrinkled stretchable nanofibrous membrane for high performance wearable triboelectric nanogenerator," *Nano Energy*, vol. 67, Article ID 104206, 2020.

[7] X. Chen, H. Huang, L. Pan, T. Liu, and M. Niederberger, "Fully integrated design of a stretchable solid-state lithium-ion full battery," *Advanced Materials*, vol. 31, no. 43, Article ID 1904648, 2019.

[8] Y.-h. Zhu, S. Yuan, D. Bao et al., "Decorating waste cloth via industrial wastewater for tube-type flexible and wearable sodium-ion batteries," *Advanced Materials*, vol. 29, no. 16, Article ID 1603719, 2017.

[9] H. Tang, W. Li, L. Pan et al., "A robust, freestanding MXene-sulfur conductive paper for long-lifetime Li-S batteries,"

Advanced Functional Materials, vol. 29, no. 30, Article ID 1901907, 2019.

[10] K. Chen, H. Huang, L. Pan, T. Liu, and M. Niederberger, "Fully integrated design of a stretchable solid-state Lithium-Ion full battery," *Advanced Materials*, vol. 31, no. 43, Article ID 1904648, 2019.

[11] J. Wu, K. Jiang, G. Li, Z. Zhao, Q. Li, and F. Geng, "Molecularly coupled two-dimensional titanium oxide and carbide sheets for wearable and high-rate quasi-solid-state rechargeable batteries," *Advanced Functional Materials*, vol. 29, no. 30, Article ID 1901576, 2019.

[12] M. K. Hota, Q. Jiang, Z. Wang, Z. L. Wang, K. N. Salama, and H. N. Alshareef, "Integration of electrochemical micro-supercapacitors with thin film electronics for on-chip energy storage," *Advanced Materials*, vol. 31, no. 25, Article ID 1807450, 2019.

[13] M. Karaaslan, M. Bagmanci, E. Unal, O. Akgol, O. Altintas, and C. Sabah, "Broad band metamaterial absorber based on wheel resonators with lumped elements for microwave energy harvesting," *Optical and Quantum Electronics*, vol. 50, no. 5, 2018.

[14] M. Bagmanci, M. Karaaslan, O. Altintas, F. Karadag, E. Tetik, and M. Bakir, "Wideband metamaterial absorber based on CRRs with lumped elements for microwave energy harvesting," *Journal of Microwave Power & Electromagnetic Energy*, vol. 52, no. 1, pp. 45–59, 2018.

[15] A. Galoic, B. Ivsic, D. Bonefacic, and J. Bartolic, "Wearable energy harvesting using wideband textile antennas," in *Proceedings of the 2016 10th European Conference on Antennas and Propagation (Eucap)*, Davos, Switzerland, April 2016.

[16] H. Li, Z. Tang, Z. Liu, and C. Zhi, "Evaluating flexibility and wearability of flexible energy storage devices," *Joule*, vol. 3, no. 3, pp. 613–619, 2019.

[17] J. Wang, G. Yang, J. Chen et al., "Flexible and high-loading lithium-sulfur batteries enabled by integrated three-in-one fibrous membranes," *Advanced Energy Materials*, vol. 9, no. 38, Article ID 1902001, 2019.

[18] X. Li, J. Zhou, J. Zhang et al., "Bamboo-like nitrogen-doped carbon nanotube forests as durable metal-free catalysts for self-powered flexible Li-co 2 batteries," *Advanced Materials*, vol. 31, no. 39, Article ID 1903852, 2019.

[19] N. Zhang and X. Zhang, "Asymmetric ring millimeter wave microstrip antenna based on communication satellite," *Foreign Electronic Measurement Technology*, vol. 32, no. 6, pp. 79–82, 2013.

[20] J. O. Mcspadden, L. Lu Fan, and K. Kai Chang, "Design and experiments of a high-conversion-efficiency 5.8-GHz rectenna," *IEEE Transactions on Microwave Theory and Techniques*, vol. 46, no. 12, pp. 2053–2060, 1998.

[21] V. Marian, C. Vollaire, and B. Allard, "Low power rectenna topologies for medium range wireless energy transfer," in *Proceedings of the European Conference on Power Electronics & Applications*, IEEE, Lille, France, 2011.

[22] A. Dolgov, R. Zane, and Z. Popovic, "Power management system for online low power RF energy harvesting optimization," *IEEE Transactions on Circuits and Systems I: Regular Papers*, vol. 57, no. 7, pp. 1802–1811, 2010.

[23] F. Jia, *Study on Preparation and Related Mechanism of Thermoelectric Materials and Micro Thermoelectric Generator Based on Electrochemical Technology*, Tianjin University, Tianjin, China, 2006.

[24] I. Boniche and D. P. Arnold, "Micromachined radial thermoelectric modules for power generation using hot gas streams," *Journal of Microelectromechanical Systems*, vol. 20, no. 2, pp. 512–521, 2011.

[25] Z. Wang, *Power Electronics*, China Machine Press, Beijing, China, 2011.

[26] Z. Cao, C. Wang, M. Yuan, J. Luo, and J. Zhang, "Research status and development trend of environmental energy acquisition technology," *Journal of Nanjing University of Posts and Telecommunications*, vol. 36, no. 4, pp. 1–10, 2016.

[27] X. Dai, S. Song, W. Xu, Z. Huang, and D. Gong, "Modal space neural network compensation control for Gough-Stewart robot with uncertain load," *Neurocomputing*, vol. 449, pp. 245–257, 2021.

[28] C. Yang, D. Huang, W. He, and L. Cheng, "Neural control of robot manipulators with trajectory tracking constraints and input saturation," *IEEE Transactions on Neural Networks and Learning Systems*, vol. 32, no. 9, pp. 4231–4242, 2021.

[29] C. Yang, C. Chen, W. He, R. Cui, and Z. Li, "Robot learning system based on adaptive neural control and dynamic movement primitives," *IEEE Transactions on Neural Networks and Learning Systems*, vol. 30, no. 3, pp. 777–787, 2019.

[30] G. Peng, C. L. P. Chen, and C. Yang, "Neural networks enhanced optimal admittance control of robot-environment interaction using reinforcement learning," *IEEE Transactions on Neural Networks and Learning Systems*, pp. 1–11, 2021.